Effects of a Warm Oceanic Feature on Hurricane Opal

LYNN K. SHAY

Division of Meteorology and Physical Oceanography, Rosenstiel School of Marine and Atmospheric Science, University of Miami, Miami, Florida

GUSTAVO J. GONI

Physical Oceanography Division, National Oceanic and Atmospheric Administration, Atlantic Oceanographic and Meteorological Laboratories, Miami, Florida

PETER G. BLACK

Hurricane Research Division, National Oceanic and Atmospheric Administration, Atlantic Oceanographic and Meteorological Laboratories, Miami, Florida

(Manuscript received 24 September 1998, in final form 21 February 1999)

ABSTRACT

On 4 October 1995, Hurricane Opal deepened from 965 to 916 hPa in the Gulf of Mexico over a 14-h period upon encountering a warm core ring (WCR) in the ocean shed by the Loop Current during an upper-level atmospheric trough interaction. Based on historical hydrographic measurements placed within the context of a two-layer model and surface height anomalies (SHA) from the radar altimeter on the TOPEX mission, upper-layer thickness fields indicated the presence of two warm core rings during September and October 1995. As Hurricane Opal passed directly over one of these WCRs, the 1-min surface winds increased from 35 to more than 60 m s^{-1}, and the radius of maximum wind decreased from 40 to 25 km. Pre-Opal SHAs in the WCR exceeded 30 cm where the estimated depth of the 20°C isotherm was located between 175 and 200 m. Subsequent to Opal's passage, this depth decreased approximately 50 m, which suggests upwelling underneath the storm track due to Ekman divergence.

The maximum heat loss of approximately 24 Kcal cm^{-2} relative to depth of the 26°C isotherm was a factor of 6 times the threshold value required to sustain a hurricane. Since most of this loss occurred over a period of 14 h, the heat content loss of 24 Kcal cm^{-2} equates to approximately 20 kW m^{-2}. Previous observational findings suggest that about 10%–15% of upper-ocean cooling is due to surface heat fluxes. Estimated surface heat fluxes based upon heat content changes range from 2000 to 3000 W m^{-2} in accord with numerically simulated surface heat fluxes during Opal's encounter with the WCR. Composited AVHRR-derived SSTs indicated a 2°–3°C cooling associated with vertical mixing in the along-track direction of Opal except over the WCR where AVHRR-derived and buoy-derived SSTs decreased only by about 0.5°–1°C. Thus, the WCR's effect was to provide a regime of positive feedback to the hurricane rather than negative feedback induced by cooler waters due to upwelling and vertical mixing as observed over the Bay of Campeche and north of the WCR.

1. Introduction

Recent cases have demonstrated that sudden unexpected intensification in tropical cyclones often occurs within 24–48 h of striking the coast upon passing over warm, oceanic regimes such as the Gulf Stream, Florida Current, and Loop Current or large, warm core rings (WCRs) in the western North Atlantic Ocean and Gulf of Mexico. Sea surface temperatures (SSTs) exceeding 26°C are a necessary, but insufficient, condition with respect to the ocean's influence on the tropical cyclone intensity changes (i.e., pressures and winds). Namias and Canyan (1981) noted that patterns of lower-atmospheric anomalies are more consistent with the upper-ocean thermal structure variability than with just SSTs. Within this context, temperatures distributed over the oceanic planetary boundary layer (OPBL), defined as the well-mixed upper-ocean layer, may be a more effective means of assessing oceanic regimes where tropical cyclone intensification is likely to occur. In the presence of warm baroclinic features, the OPBL and the depth of the warm isotherm (≈26°C) are much deeper and represent regions of positive feedback to the atmosphere.

Corresponding author address: Dr. Lynn K. Shay, Division of Marine and Physical Oceanography, Rosenstiel School of Marine and Atmospheric Science, 4600 Rickenbacker Causeway, Miami, FL 33149.
E-mail: nick@rsmas.miami.edu

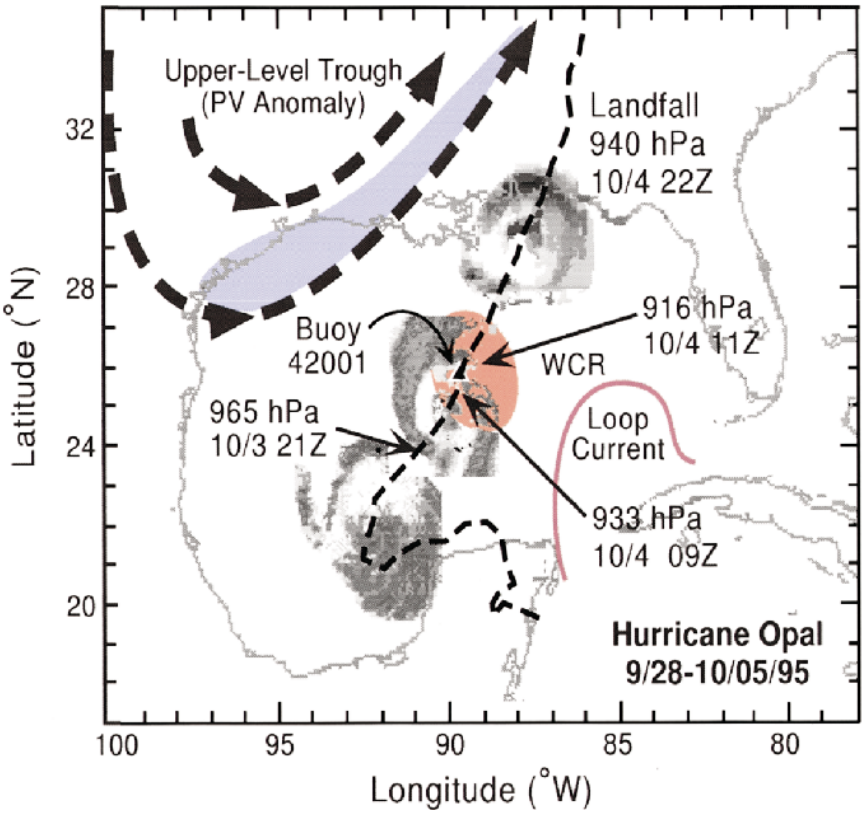

FIG. 1. Position of upper-level trough and location of Loop Current WCR based upon TOPEX altimetry data and poststorm AVHRR images relative to the position of Hurricane Opal's track in the Gulf of Mexico from 28 Sep to 5 Oct 1995 (adapted from Marks et al. 1998).

From a climate perspective, one of the best-known circulation systems in the world's ocean is the North Atlantic subtropical gyre, which includes the Gulf Stream, Florida Current, and Loop Current, as well as warm and cold core rings. On a near-annual basis, warm water is transported from the Caribbean Sea into the Gulf of Mexico through the Yucatan Straits, and then forces the Loop Current (Fig. 1). This anticyclonic rotating current with maximum flows of 1–2 m s^{-1} intrudes 500 km northward into the Gulf of Mexico and transports subtropical water with markedly different temperatures and salinities compared to the background Gulf of Mexico water between ocean temperatures of 18°–26°C (Shay et al. 1998). Since the depth of the 20°C isotherm is between 180 and 220 m in the subtropical water compared to less than 100 m in the Gulf common water, these deeper, warmer subtropical waters increase the heat potential of the Loop Current and also represent a significant contribution to oceanic mesoscale variability in the Gulf of Mexico. As this feature intrudes farther north, WCRs having horizontal length scales of *O*(200 km; Elliot 1982) pinch off from the Loop Current at 11–14-month intervals, propagate westward with speeds between 1 and 14 km day^{-1} (Maul 1977; Vukovich and Crissman 1986) over a 9–12-month period, and eventually dissipate along the shelf break off Texas and Mexico.

Warm current regimes border the coastlines along the United States eastern seaboard and Gulf of Mexico states, and provide additional heat sources for the passage of tropical and extratropical cyclones that may lead to intensity change (Black and Shay 1998). Quantifying the effects of these oceanic features on changes in the surface pressure and wind field during tropical cyclone passage has far-reaching consequences not only for the research and forecasting communities, but also for the public who rely on the most advanced forecasting systems to prepare for landfall. Given the unprecedented tropical cyclone activity in the Atlantic Ocean basin during recent seasons, and the nearly exponential growth in coastal populations (Pielke and Pielke 1997), the influence of warm upper-ocean processes on the atmospheric planetary boundary layer (APBL) has to be assessed with respect to surface wind field changes in hurricanes to advance our understanding of these processes (Marks et al. 1998).

During Hurricane Opal's intense deepening phase from 965 to 916 hPa over 14 h on 3 October 1995 (Fig. 1), the maximum 1-min surface winds, estimated from reconnaissance flights, increased from 35 to more than

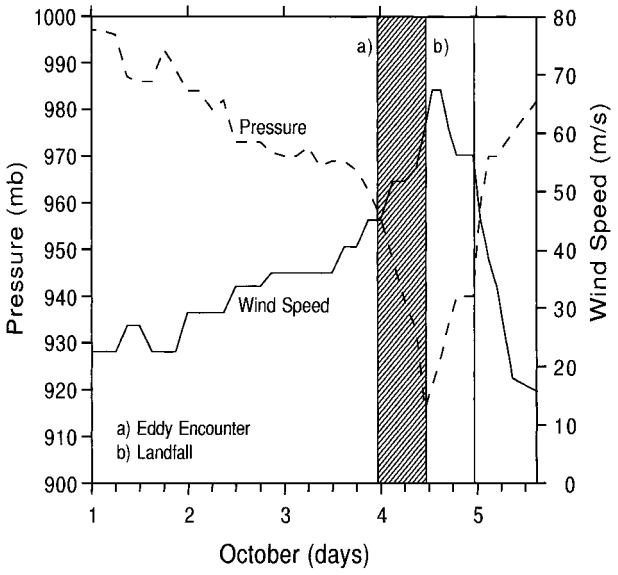

FIG. 2. Estimated 1-min wind speed (solid) in m s^{-1} and sea level pressure in mb (dashed) from 1 to 5 Oct associated with Hurricane Opal relative to the WCR encounter (a: shaded area) and landfall (b) from the advisories and reconnaissance missions.

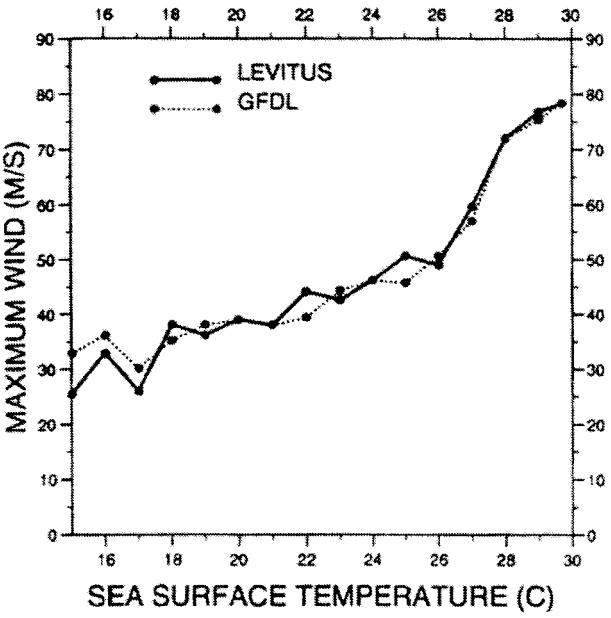

FIG. 3. Maximum storm intensity for each 1°C group for 1962–88 sample with Levitus climatological SST and GFDL monthly SST analyses (from DeMaria and Kaplan 1994). Note the sharp rise in maximum winds beyond 26°C.

60 m s^{-1} as shown in Fig. 2. According to Bosart et al. (2000), Opal was at least 15 m s^{-1} below its maximum potential intensity prior to this deepening event based upon theoretical arguments (Emanuel 1986; Holland 1997). Further, vertical current shear in the upper atmosphere was relatively weak (2–3 m s^{-1}); and, as the cyclonic spinup of Opal was maximized due to the approaching trough from the northwest, atmospheric conditions were favorable for this intense deepening cycle starting 2000 UTC 3 October. A series of Special Sensor Microwave/Imager (SSM/I) images indicated the presence of a well-developed eye as R_{max} decreased from 40 to about 25–30 km. In this area of Opal's deepening, the prestorm SST distribution in the Gulf of Mexico showed no apparent signs of a WCR as Advanced Very High Resolution Radiometer (AVHRR) derived SSTs exceeding 29°C were uniformly distributed due to strong solar heating occurring during the summer months in the Gulf of Mexico (Shay et al. 1992). Skin temperatures tend to be 0.5°–0.7°C higher than the underlying OPBL temperatures. However, images from the National Aeronautics and Space Administration (NASA) oceanographic Topography Experiment (TOPEX) mission and poststorm AVHRR-derived SST from National Oceanic and Atmospheric Administration (NOAA-10 and -12) satellites suggested that during this time Opal passed over a WCR. Subsequently, the rapid intensification ended about 1000 UTC 4 October as Opal exited the WCR regime and encountered a shallower OPBL and strong vertical shear in the atmospheric layer from 200 to 850 mb as noted by Bosart et al. (2000).

Whereas Bosart et al. (1999) document the favorable atmospheric conditions associated with trough interactions, the approach described herein focuses on the upper ocean's role in altering the tropical cyclone wind fields as Hurricane Opal passed directly over the WCR. Accordingly, air–sea interaction processes will be described in section 2 including buoy measurements from National Data Buoy Center (NDBC) buoy 42001, followed by a two-layer model treatment where the vertical ocean structure is divided into an upper and lower layer based upon the depth of the 20°C isotherm (section 3). Hydrographic measurements are combined with remotely sensed signals from TOPEX and AVHRR to provide synoptic assessments of upper-layer thicknesses and upper-ocean heat content relative to the 26°C isotherm in section 4. Concluding remarks concerning the application of these fields to Opal and the general approach to the intensity change problem are discussed in section 5.

2. Air–sea interaction processes

Palmen (1948) originally noted that warm, preexisting SSTs in excess of 26°C are a necessary, yet insufficient, condition for tropical cyclogenesis. Once a tropical cyclone develops and translates over the tropical oceans, DeMaria and Kaplan (1994) (Fig. 3) found that climatological SSTs (actually OPBL temperatures) describe a large fraction of the variance (40%–70%) associated with wind speed increases. However, these statistical models neither account for the layer depths where temperatures exceed the 26°C threshold, nor for the thermal advective tendencies by basic-state oceanic currents. In the Loop Current and Gulf Stream regimes,

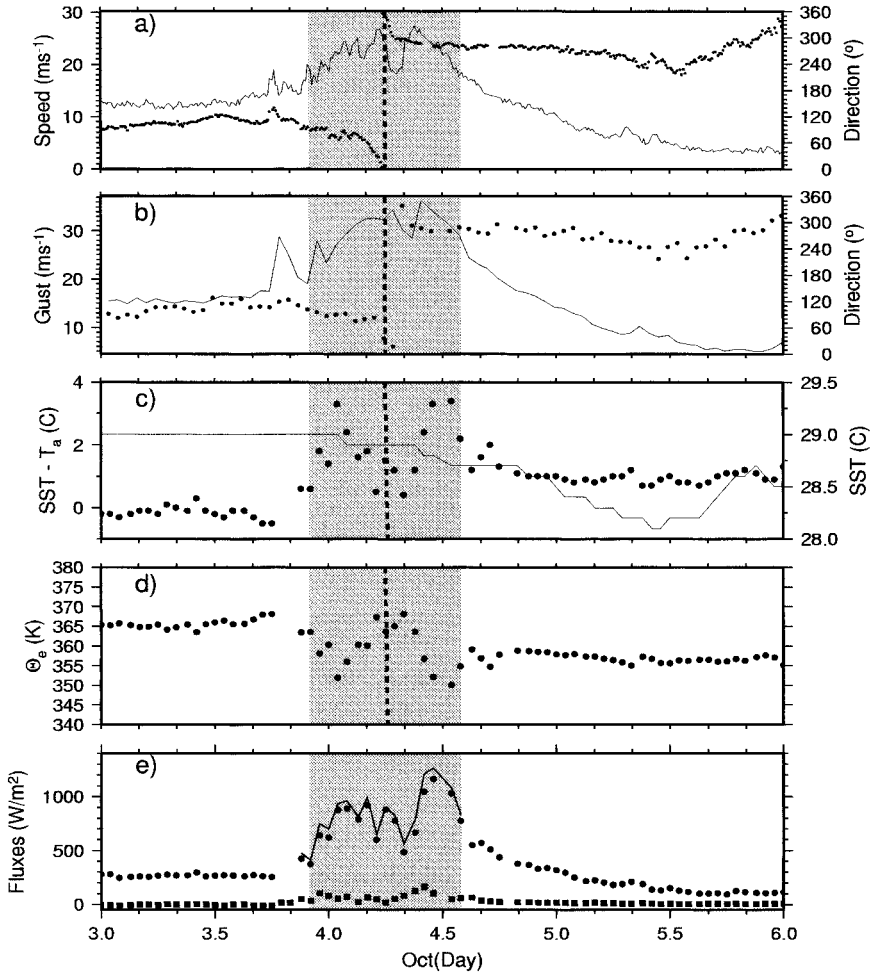

FIG. 4. Time series of (a) wind speed (solid, m s^{-1}) and direction (dashed, °) for 10-min records, hourly (b) wind gusts (solid, m s^{-1}) and direction (circles, °), (c) SST-T_a (circles) and SST (solid) both in °C, (d) θ_e (K), and (e) latent (circles), sensible (squares), and total (solid line during Opal) heat fluxes (W m^{-2}) from NDBC buoy 42001 located on the left side of the Opal's track in the WCR. Note that a relative humidity of 85% was assumed in these estimates with wind speed–dependent bulk coefficients. The gray area approximates Opal's closest approach to the buoy and the vertical black line is the time of the lowest surface pressure of 963 mb.

current velocities range from 1 to 2 m s^{-1} and advect deep, warm upper-ocean layers that represent reservoirs of high-heat content water and locations where enhanced surface heat fluxes during tropical cyclone passage occur.

a. Atmospheric response

As shown in Fig. 1, the behavior of the 10-min, surface winds suggest that the NDBC buoy 42001 (a 10-m discus buoy) was located in the eyewall (25°55′N, 89°39′W) on the left side of Opal's track during its encounter with the WCR. There were two increases in the surface winds as the maximum surface winds approached 28 m s^{-1}. This wind speed maximum was about 17 m s^{-1} less than those inferred from the right side of the track due to the asymmetry induced by translation speed (Fig. 4a). Notice that the wind gusts exceeded 30 m s^{-1} during the storm (Fig. 4b). Perhaps the more important aspect here is that the SST and air temperature (T_a) differences ranged between 2° and 4°C at the buoy (Fig. 4c). The SSTs were larger than the surrounding air temperatures beginning between 1800 UTC 3 October and ending 1400 UTC 4 October. Prestorm SSTs were 29°C, which is normal for the Gulf of Mexico for this time of the year, and decreased by about 0.5°C as shown in the poststorm temperatures. A clearer indication of the air–sea interaction process and the atmospheric response to the oceanic forcing is the equivalent potential temperature (θ_e), estimated by assuming a relative humidity of 85% following Bohren and Albrecht (1998). Consistent with estimates from obser-

TABLE 1. Air–sea parameters, nondimensional numbers, and scales in Hurricane Opal based upon Price's (1983) scaling arguments. Note that the drag coefficient was estimated using a constant value of 3.775×10^{-3} based upon internal wave fluxes in Gilbert (Shay 1997) and the drag coefficient found by the WAMDI Group (1988).

Parameter		
Radius of max winds (km)	$R_{\max}$	25
Max wind stress (N m^{-2})	$\tau_{\max}$	9.8 (10.3)
Speed of the hurricane (m s^{-1})	U_h	8.5
Wavelength (km)	Λ	860
First mode phase speed (m s^{-1})	c_1	3.0
First mode deformation radius (km)	α_n^{-1}	47
Inertial period (days)	IP	1.14
Nondimensional numbers		
Froude number (Fr)	(U_h/c_1)	2.8
Nondimensional storm speed (S)	$(U_h/2R_{\max}f)$	2.65
Nondimensional forcing (Fo)	$2R_{\max}/\alpha_1$	1.06

vational studies (Black 1983; Cione et al. 2000), the maximum θ_e was as high as 365 K in the eyewall as shown in Fig. 4d. This value agreed with observations (Bosart et al. 2000) and simulations (Hong et al. 2000). Using a wind speed–dependent bulk aerodynamic formula (Fig. 4e), latent heat flux ranged between 300 and 1200 W m^{-2} m^{-2} whereas sensible heat flux was a maximum of 200 W m^{-2}. Note that during this time of intense forcing, the maximum total surface heat flux exceeded 1270 W m^{-2}, which was within the envelope defined by (Cione et al. 2000). On the right side of the storm where winds approached 50 m s^{-1} during the intensification phase (farther north of the buoy), the fluxes would be nearly double as suggested by numerical simulations of Hong et al. (2000).

b. Air–sea variables

The oceanic response to tropical cyclones is set by the atmospheric forcing scales and key air–sea variables. Scaling arguments of Price (1983) and Greatbatch (1983) are used to place the predicted upper-ocean response into a nondimensional framework. The oceanic wavelength of the response induced by a moving tropical cyclone is proportional to the product of the storm translation speed (U_h) and the inertial period (IP; Geisler 1970). Based upon an 8.5 m s^{-1} translation speed for Opal over the WCR ($\approx$00Z 4 October) and an IP of 27.4 h, the predicted wavelength (Λ) is estimated to be 838 km with an uncertainty of $\pm$60 km (Table 1).

Isotherm displacements (ξ), induced by time-dependent Ekman pumping associated with the wind stress curl, scale as $\tau_{\max}/\rho_o f U_h$ or about 22–24 m for surface wind stress of 9.8–10.3 N m^{-2}. Based upon the wind speed–dependent drag coefficients from the WAMDI Group (1988), and more recently Shay (1997), the surface wind stress in the Opal cases was larger than in the usual cases for tropical cyclones where surface winds typically range from 35 to 40 m s^{-1}. Since Opal's near-surface winds increased to 47–50 m s^{-1}, the wind stress and the wind speed–dependent drag coefficients were quite large in comparison to these more typical cases. Moreover, this relationship indicates that as the storm speeds decrease, there is an increase in the displacements. One day earlier when Opal's translation speed was considerably less, the vertical displacement of the isotherms was larger as upwelling of cooler water from a shallower thermocline (i.e., in the Gulf common water) was detected. For a nearly stationary storm, a WCR may be significantly weakened by persistent upwelling of the thermocline water to the surface over a few day period as found in Hurricane Anita in 1977 (Black 1983) and more recently in Hurricane Mitch in 1998.

As a tropical cyclone moves over these warm current regimes at moderate to fast speeds, the time available for vertical mixing (L/U_h, where U_h is the storm speed and L represents the curl of the near-surface wind stress or approximately $\pm 2R_{\max}$ is short compared to the inertial period (f^{-1}-inertial timescale) (Greatbatch 1983). The relevant scale of the strong wind stress curl, based upon a series of SSM/I data, was about 120 km ($R_{\max} \approx 30$ km). Thus, the time available for vertical mixing was about 4 h compared to the local inertial period of 27.4 h equating to a ratio of 1:7. This ratio suggests that the upper ocean had little time to vertically mix and cool during Opal's rapid acceleration phase. A second important aspect is that a source of warm ocean water, advected by an energetic current, provides a nearly continuous source of heat and moisture for moderate to fast moving (5–10 m s^{-1}) tropical cyclones. That is, horizontal heat advection by the geostrophically balanced currents has an important effect on the three-dimensional upper-ocean heat balance as well as vertical mixing processes at OPBL base (Jacob et al. 2000). The combination of these two oceanic effects may have led to significant increases in the surface wind field that devastated South Florida coastal communities during Hurricane Andrew in 1992 (Powell and Houston 1996).

c. SSTs

A common perception of air–sea coupling in tropical cyclones is that SST represents the only important oceanic parameter for the maintenance of tropical cyclones (Palmen 1948). To illustrate that OPBL temperatures are important, a highly idealized case is considered where the surface buoyancy flux is set to zero in a one-dimensional, deepening mixed layer based upon Kraus and Turner (1967) given by

$$\frac{dh}{dt} = \frac{1}{\Delta T}\left[\frac{2}{\alpha g h}\left(\frac{\rho_a c_d}{\rho_o}\right)^{3/2} W^3\right], \tag{1}$$

where h is the OPBL depth, ΔT is the temperature difference between an AVHRR-derived SST and the underlying OPBL temperature of 0.6°C (Shay et al. 1992), α is the thermal expansion coefficient (2.5×10^{-4} °C^{-1}),

TABLE 2. Time required (h) to erode a shallow layer with temperatures 0.6°C greater than the underlying mixed layer temperature as a function of wind speeds as per (1).

Depth (m)	4 m s^{-1}	7 m s^{-1}	10 m s^{-1}
0.5	0.40	0.07	0.03
1.0	1.60	0.30	0.10
3.0	14.40	2.70	0.92

g is the acceleration of gravity (9.81 m s^{-2}), ρ_o is the water density (1.026 $\times$ 10^3 kg m^{-3}), ρ_a is the air density (1.2 kg m^{-3}), c_d is the drag coefficient (1.3 $\times$ 10^{-3}), and W is the surface wind speed.

This simple model is used to solve for the time required for nominal wind speeds of 4–10 m s^{-1} to erode thin SST layers of thicknesses 0.5 m, 1 m, and 3 m that overlie an OPBL.[1] For a ΔT of 0.6°C, the time required to erode the thin layer from a AVHRR image is a fraction of an hour even for a 4 m s^{-1} wind speed (Table 2). In fact, AVHRR-derived SSTs represent a thin layer of temperatures less than a few millimeters thick that mixes with the OPBL water quickly for winds of this magnitude. If the 3-m depth is chosen for the same wind condition, the time required to vertically mix it with the underlying well-mixed OPBL water is 15 h. As the winds increase, however, the required time to erode even a 3-m layer decreases substantially from 2.7 h for a 7 m s^{-1} wind speed to less than an hour for a 10 m s^{-1} surface wind speed. As winds increase to gale force (>17 m s^{-1}), the tropical cyclone removes heat from the OPBL. The implication here is that the underlying oceanic structure has far more importance in the heat and moisture fluxes feeding the storm than just SST as noted in previous studies (Elsberry et al. 1976; Black 1983; Shay et al. 1992). Since the degree of upper-ocean cooling is also a function of the OPBL depths, the regions of deep warm layers (i.e., WCR) will thus provide more heat to the storm than regions of shallow OPBLs (i.e., Gulf common water).

d. Oceanic vertical structure and heat content

As shown in Fig. 5, thermal structure measurements from Hurricane Gilbert from both inside and outside a WCR demonstrate the marked thermal contrast in the upper-oceanic layers. Directly along the track, the OPBL depth was about 40 m with currents of about 0.6V_{is}, where V_{is} represents the scaled wind-driven current from Gilbert of 1.07 m s^{-1} (Shay et al. 1998). At the base of the OPBL, these currents decreased and reversed direction, which created vertical current shear that drove the vertical mixing process by lowering the Richardson number, defined as Ri = $\overline{N}^2/(\mathbf{V}\cdot\mathbf{V})_z$, to below criticality. Outside the WCR (Fig. 5b), the OPBL depth was 40 m, and strong stratification, as defined by the buoyancy frequency

$$\overline{N}^2 = -\frac{g}{\rho_o}\frac{\partial\overline{\rho}}{\partial z}, \tag{2}$$

occurred at the top of the thermocline [$\overline{N} \approx 15$ cph (cycles per hour)]. By contrast, the depth of the isothermal layer in the WCR was about 60 m with fairly weak stratification ($\overline{N} \approx$ 6–8 cph). However, the strong current shear (2–3 $\times$ 10^{-2} s^{-1}) rotated clockwise with depth and induced mixing events through shear instabilities by lowering the gradient Ri to below 0.25 that deepened and cooled the OPBL.

Of prime importance is the deeper isothermal layer between 60 and 170 m in the WCR. That is, warmer water with temperatures approaching 26°C extend to greater depths than in the usual case in the Gulf common water (150 vs 50 m). These higher temperatures at depth have a significant influence on the heat content contrast between the two profiles. Outside the WCR, the heat content was 15 Kcal cm^{-2} compared to about 27 Kcal cm^{-2} within the WCR during the storm relative to 26°C. Moreover, the vertical shear at the base of the isothermal layer (≈160 m) was insufficient to induce any further layer cooling by vertical mixing as the Ri exceeded 0.25. This type of deep isothermal structure found in warm oceanic features provides more heat for atmospheric disturbances by enhanced air–sea fluxes. Based on the buoy temperatures, the net upper-ocean cooling observed in Opal was only about 0.5°C in the WCR, which is consistent with these mixing length arguments.

e. Remotely sensed ocean data

Satellite altimetry data have proven to be a useful tool to study eddy dynamics by acquiring continuous global coverage of surface height anomaly (SHA) fields. Unlike AVHRR imagery, altimeter data are unaffected by cloud obscuration and can provide information on the vertical ocean structure if complemented by historical hydrographic data. Given the relatively slow translational speeds of mesoscale ocean features of a few kilometers per day, the surface height data from the altimeter detects and locates warm mesoscale features, usually identified as positive SHA values.

The data used in this study are derived from TOPEX/Poseidon (T/P) radar altimetry. The NASA T/P altimeter was launched in 1992, orbiting the earth at an altitude of 1336 km. The altimeter directly measures the sea level beneath its ground track at 7-km intervals every 9.92 days where adjacent tracks are separated by about 3° longitude. The resulting SHA data include corrections for land and ocean tides, wet and dry tropospheric ef-

[1] By setting the surface flux to zero, the utilization of (1) is invoked for the deepening process as opposed to retreat where surface flux and wind are equated to estimate the Obukhov length scales. During storm conditions, the upward surface buoyancy flux and the surface wind act together to erode the thin SST layers even more quickly during the deepening process.

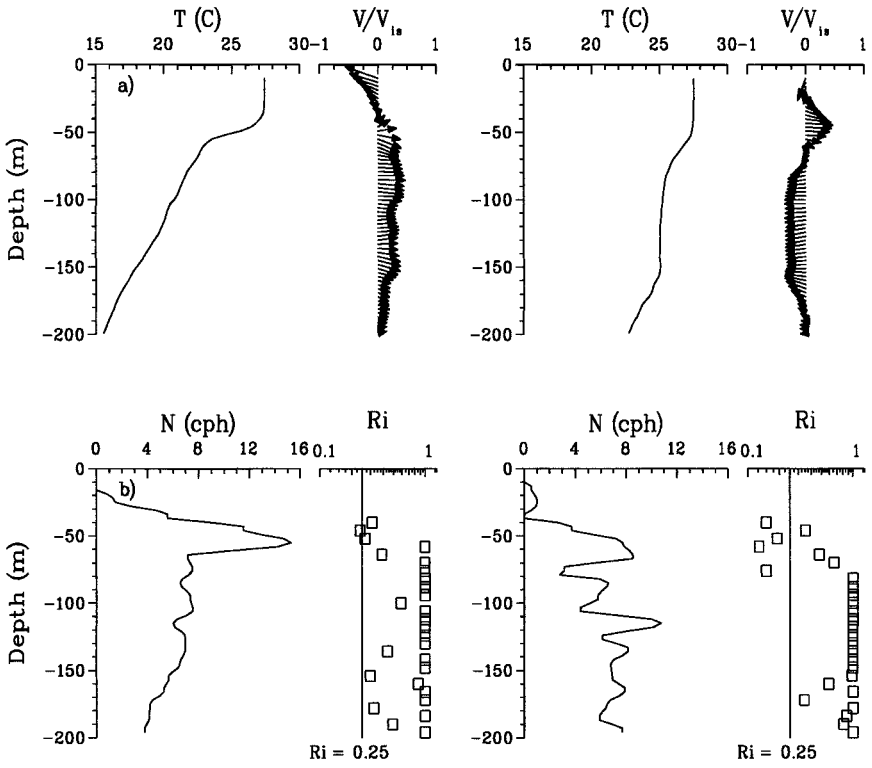

FIG. 5. Vertical structure analysis of two velocity, temperature, and density profiles from the Hurricane Gilbert measurements outside the eddy (left panels) and inside the eddy (right panels) for (a) temperature (°C) and residual velocity (observed−geostrophic) normalized by the scaled wind-driven velocity of 1.07 m s^{-1}, and (b) buoyancy frequency (cph) and gradient Richardson number where the solid line depicts the critical value of 0.25.

fects, ionospheric processes, electromagnetic bias, and inverse barometric corrections. The SHA fields represent sea level heights at each satellite alongtrack location referenced to the mean sea level heights based on 1992–97 measurements. The 7-km alongtrack SHA are subsequently smoothed using a 30-km running mean filter and interpolated into a regular 0.25° × 0.25° grid using a Gaussian interpolator with radius of interpolation of 0.4°.

Altimeter-derived SHA fields corresponding to September 1995 indicate the presence of warm features in the Gulf of Mexico prior to Opal's passage (Fig. 6a). The AVHRR-derived SSTs over the basin exceed 29°C except along the northern periphery where shelf waters have temperatures about 2°C cooler (Fig. 6b). Notice that Opal's track passes directly over the warm feature that is apparent in the poststorm AVHRR imagery and is associated with the positive SHA values where surface winds increased significantly (Figs. 6a,c). Composited SST images also indicate a 2°–3°C cooling along the hurricane track outside of the WCR (Fig. 6d). Since prestorm SSTs exceeding 29°C were distributed over the Gulf of Mexico basin, these results suggest that this cooling was induced by the oceanic mixing processes and the heat loss to the atmosphere. However, the cooling in the WCR was only 1°C or less due to the deeper, warm layers of the oceanic feature consistent with buoy measurements (Fig. 4c).

From the SHA fields, the horizontal extent of the mesoscale features is difficult to discern given the approximate 300-km distance between adjacent tracks. When both the TOPEX and AVHRR imagery are used in conjunction, a clearer depiction of the oceanic scales emerge, particularly after storm passage, when the thin SST layer derived from AVHRR is mixed with the underlying OPBL. These basic physical processes are consistent with mixing arguments, and the deep isothermal structure found in warm oceanic features that are manifested on the free surface as positive SHA, consistent with hydrostatic dynamics. To define relevant horizontal scales and locations of the WCR's center, remotely sensed data must be combined with available hydrography measurements cast into a two-layer fluid.

3. Two-layer ocean model approach

a. Upper-layer thickness

Altimeter-derived SHA data calibrated by hydrographic data (i.e., temperature and salinity) can be used as a proxy to monitor the upper-layer thickness and transport based on a two-layer model approximation

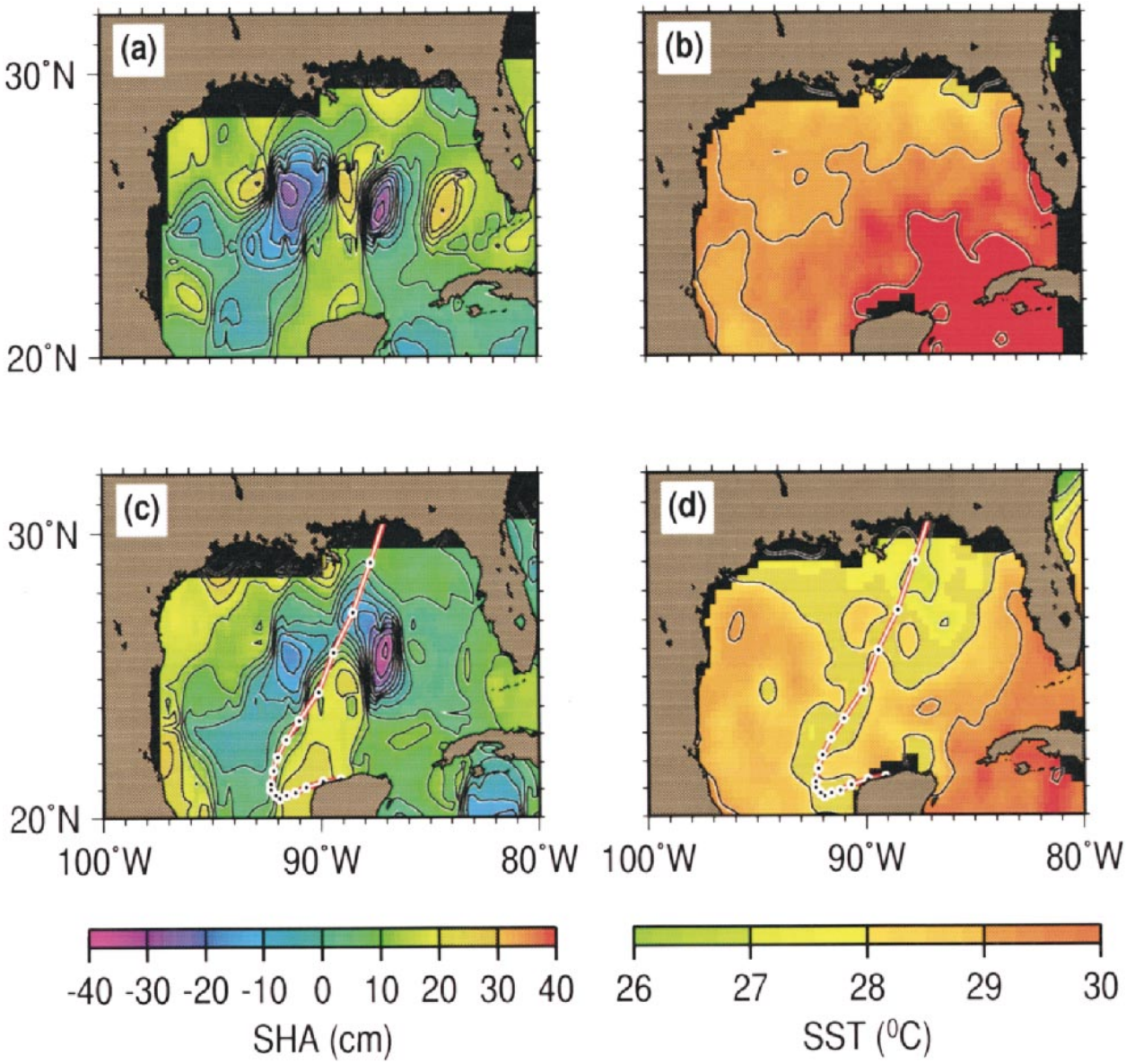

FIG. 6. (a) Prestorm altimeter-derived SHA map for cycle 111 (18–27 Sep 1995) showing positive height anomalies above 30-cm height corresponding to the WCR located on the right side of Opal's track. (b) Prestorm objectively analyzed AVHRR SST composited from 27 to 28 Sep images. (c) Poststorm altimeter-derived SHA map for cycle 113 (28 Sep–8 Oct 1995) showing positive anomalies above 10-cm height corresponding to the WCR located along Opal's track. (d) Post storm objectively analyzed AVHRR SST composited from 4 to 5 Oct 1995 showing the ocean cooling pattern induced by Opal's winds along the track (SST images courtesy of A. J. Mariano and E. H. Ryan, RSMAS Remote Sensing Group). Contour interval is 5 cm.

(Goni et al. 1996, 1997; Garzoli et al. 1997). The upper-layer thickness along with historical temperature and salinity profiles are used here to monitor the upper-layer heat content and assess oceanic heat loss during Opal's passage. Leipper and Volgenau (1972) first proposed a *hurricane heat potential*, which is a measure of oceanic heat content from the surface to the depth of the 26°C isotherm. This value is chosen since it represents a threshold temperature suggested for hurricane genesis by Palmen (1948), which corresponds to mean wet-bulb temperature. Presumably, the surface fluxes would be small below this value.

If the vertical ocean structure is approximated by a two-layer fluid, the upper-layer thickness (h_1) can be estimated from the altimeter-derived SHA (η') field, provided that the mean upper-layer thickness ($\overline{h}_1$) and reduced gravity (g') fields are known to a first order from historical measurements based upon the expression

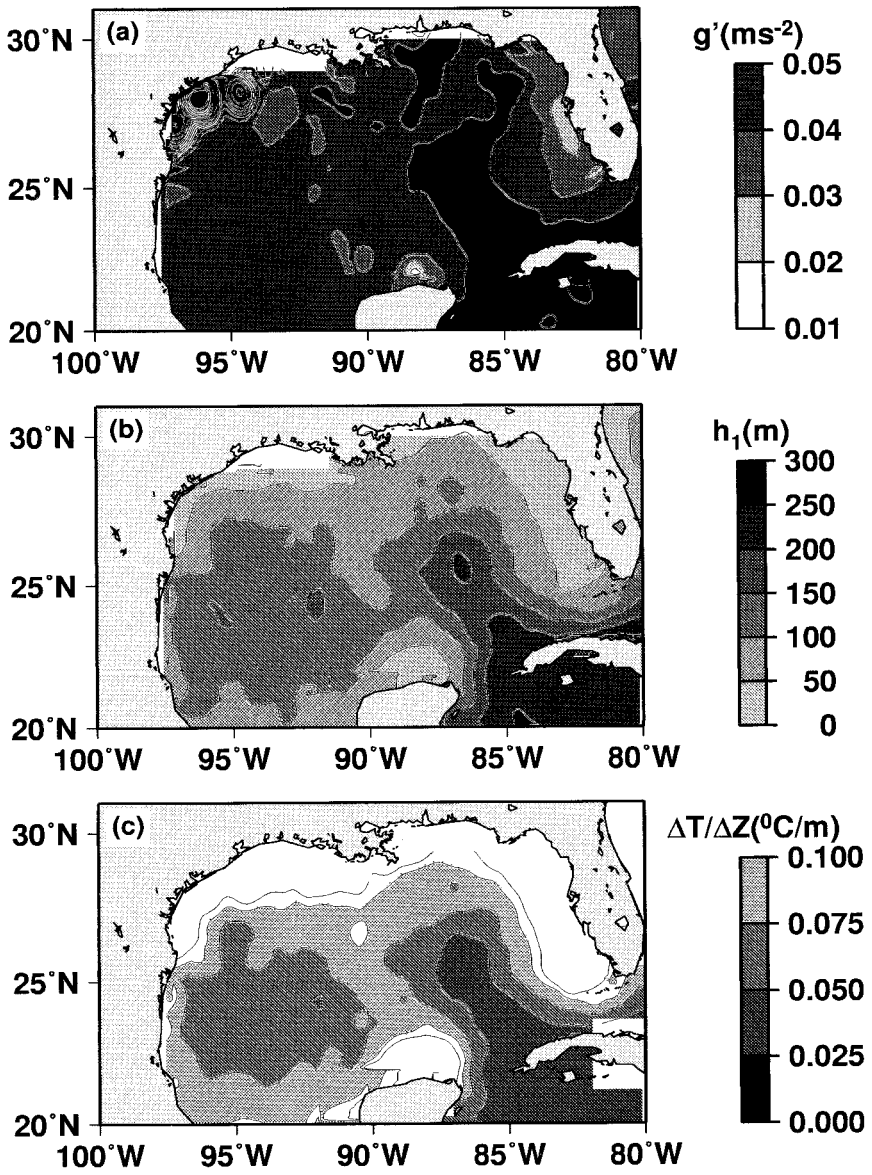

FIG. 7. (a) Reduced gravity (g′, $\times 10^{-2}$ m s^{-2}), (b) mean upper-layer thickness ($\overline{h_1}$, m), and (c) vertical temperature gradients ($\Delta T \Delta z^{-1}$, °C m^{-1}) derived from hydrographic observations in the Gulf of Mexico.

$$h_1(x, y, t) = \overline{h}_1(x, y) + \frac{g}{g'(x, y)}\eta'(x, y, t), \qquad (3)$$

where $g' = \epsilon g$, g is the acceleration of gravity, and

$$\epsilon(x, y) = \frac{\rho_2(x, y) - \rho_1(x, y)}{\rho_2(x, y)}, \qquad (4)$$

where $\rho_1(x, y)$ and $\rho_2(x, y)$ represent upper-and lower-layer densities, respectively.

The upper-layer thickness is defined from the sea surface to the depth of the 20°C isotherm. Early studies of the vertical structure of fronts and rings in the Gulf of Mexico show that the largest vertical temperature gradients are located between 15° and 21°C (e.g., Elliot 1982; Vukovich and Crissman 1986; Cooper et al. 1990). Based upon temperature and salinity variability from hydrographic measurements, the choice of the 20°C isotherm depth is deemed appropriate for the assumed two-layer ocean in this analysis. That is, the 20°C isotherm separates two layers of differing densities inside and outside the warm core rings (see Fig. 4 in Shay et al. (1998).

Climatology based upon Levitus (1984) is used to estimate reduced gravity (g') and mean upper-layer thickness ($\overline{h}_1$) as shown in Fig. 7. The values of reduced gravities (Fig. 7a) range from 2 to 6 $\times$ 10^{-2} m s^{-2},

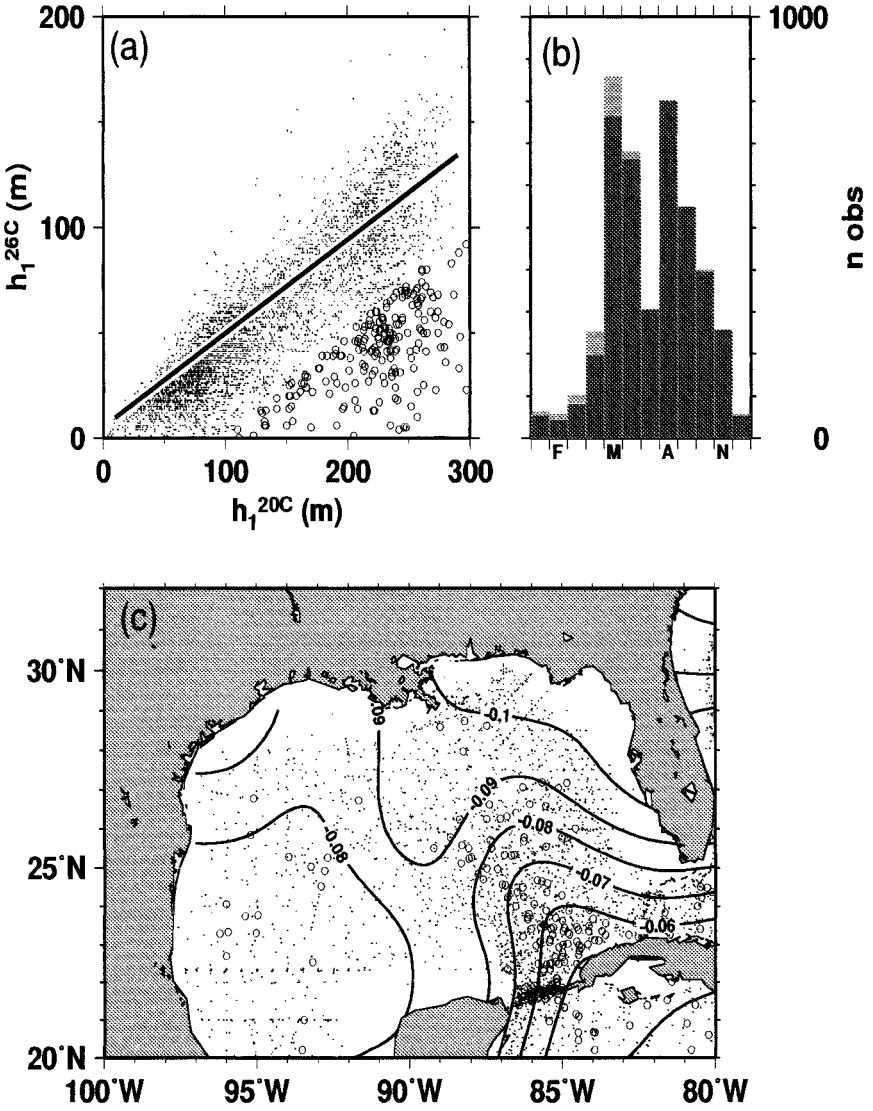

FIG. 8. (a) Regression analysis of the depth of the 20°C isotherm vs the depth of the 26°C isotherm based on hydrographic measurements in the Gulf of Mexico. The best line fit is represented by the solid line. (b) Number of hydrographic observations vs month. The lighter gray boxes represent the outliers in (a). (c) Spatial distribution of the hydrographic measurements and the contoured vertical temperature gradient between the 20° and 26°C isotherms.

suggesting a stratified ocean. Larger values of reduced gravities are associated with the core of the Loop Current, and the fresher water influx from the Mississippi River Delta along the shelf in the northern part of the basin. Notice the deeper layer thicknesses exceeding 100 m are aligned with the axis of the Loop Current along 85°W. The maximum upper-layer thickness in the Loop Current exceeds 200 m just north of the Yucatan Straits, consistent with previous studies (Maul 1977; Vukovich and Crissman 1986). The vertical temperature gradient (Fig. 7c) reveals weaker thermal structure in the core of the Loop Current where the reduced gravity values are the largest. Thus, this result underscores the importance of the effect on salinity in defining subtropical water density. During the periods of maximum penetration of the Loop Current north of the Yucatan Straits, WCRs are formed by current instabilities. The resulting WCRs have horizontal scales of 180–220 km and propagate west to southwest at rates between 1 and 14 km day^{-1} (Vukovich and Crissman 1986).

b. Vertical ocean structure

Hydrographic data from 5000 stations in the Gulf of Mexico are used to determine an empirical relationship between the depth of the upper-layer thicknesses (i.e.,

depth of the 20°C isotherm) and the depth of the 26°C isotherm (hereafter referred to as H), which is more relevant for hurricanes (Palmen 1948; DeMaria and Kaplan 1994). As a first approximation, a linear regression is made between H and h_1, yielding a relationship where the upper-layer thickness is approximately twice the depth of the 26°C isotherm (Fig. 8a):

$$H(x, y, t) = 0.48h_1(x, y, t) - 5. \quad (5)$$

This linear regression (units of m) is correlated at a level of 0.77 over most of the Gulf of Mexico. A large fraction (≈98%) of the data is within one standard deviation from the regression line. Profile data, based upon the criteria $h_1 > 0.5(H - 100)$, are neglected (outliers) in the analysis as depicted as circles in Fig. 8a. This procedure allows the conversion of the upper-layer thickness field relative to h_1 based on the two-layer model to maps of H. A large fraction of the hydrographic data was acquired between the months of April and November, with a majority of the outliers (lighter gray bars in Fig. 8b) occurring during the months of April and May. Contoured vertical temperature gradients between the surface and H (Fig. 8c) are also required to obtain the heat content estimates. Given the large separation between these two depths within this current field, these gradients are smaller inside the core of the Loop Current. Outside of these warm features, the stratification is larger in the Gulf common water because of the shorter distance between the sea surface and H suggested by Fig. 5a.

c. Oceanic heat content

The depth to which the temperature exceeds 26°C is proportional to the hurricane heat potential (Leipper and Volgenau 1972). This definition is arbitrary in the sense that the average T_a is typically 24°–26°C. In warm baroclinic structures, the 26°C water is distributed over deep layers ranging from 80 to 120 m deep. Leipper and Volgenau (1972) defined heat content of the upper layer relative to the depth of the 26°C isotherm:

$$Q(x, y, t) = \rho c_p \Delta T(x, y, t)\Delta z(x, y, t), \quad (6)$$

where ρ is the average oceanic density taken as 1.026 g cm^{-3}, c_p is the specific heat at constant pressure taken as 1 cal gm^{-1} °C^{-1}, and ΔT is the difference between the SST and 26°C summed over a depth interval Δz. If vertical structural measurements are available at a given depth interval, the heat content expression is easily solved. However, in situ thermal and momentum structure observations are not always available, and in the summer months one of the setbacks is the spatially uniform AVHRR-derived SSTs above 29°C with little thermal contrast in the Gulf of Mexico (see Fig. 6b). From a bulk perspective, if Δz is taken as H, the depth of the 26°C isotherm, then (6) becomes

$$Q(x, y, t) = \rho c_p \nabla_z T(x, y) H^2(x, y, t), \quad (7)$$

where $\nabla_z T$ is the mean vertical temperature gradient between the surface and the 26°C isotherm obtained from AVHRR-derived SSTs and historical hydrographic data (Fig. 8c).

4. Oceanic structure inferred from remotely sensed signatures

a. Pre-Opal

The altimeter-derived SHA field for the T/P cycle 111, corresponding to the period 18–28 September 1995 shown in Fig. 9a, represents the conditions prior to the passage of hurricane Opal (pre-Opal). Two distinct areas of positive SHA occur at 26°N and 88°W and 94°W, which are associated with westward propagating WCRs and the Loop Current. Although, WCRs are usually associated with positive SHA values, the opposite is not always true as discussed by Goni et al. (1996). In this specific case, alternating large positive and negative SHAs east of 90°W indicate the presence of WCRs and the edge of the Loop Current, respectively. These phenomena are observed in the upper-layer thickness maps constructed using (3) as shown in Fig. 9b. The locations of the Loop Current and of two WCRs, hereafter referred to WCR A and B, are depicted in the same figure. The estimated maximum upper-layer thicknesses of WCR A and B during cycle 111 are approximately 200 m and 150 m relative to 20°C isotherm depth, respectively. The estimated heat content within WCR A during cycle 111 was a maximum of 55 Kcal cm^{-2} located within the core of the WCR as shown in Fig. 9c. The heat content within WCR B has a maximum value of 35 Kcal cm^{-2}.

b. Post-Opal

The altimeter-derived SHA field for the TOPEX cycle 113, which corresponds to the period 8–17 October 1995, that is, 4–13 days after Opal's passage (post-Opal), is shown in Fig. 10a. The decrease of 20 cm in the SHA field along the hurricane track is due in part to the net heat lost to the hurricane, and the wind stress curl that forces a barotropic trough on the free surface. For example, Shay and Chang (1997) found that after the passage of a Hurricane Frederic an elongated depression of 22 cm in geostrophic balance remained in the cold wake of the storm. The decrease in upper-layer thickness is presumably due to upwelling close to track via Ekman pumping (Fig. 10b). Additionally, the time available for vertical mixing is short compared to the local inertial period, and the upper-layer thickness in the WCR is quite large (>100 m). If the storm slows down or becomes stationary over a WCR, the structure may be weakened due to the strong upwelling as observed in Hurricane Anita (Black 1983). Post-Opal hurricane heat content is a maximum of about 30 Kcal cm^{-2} in the northern part of WCR A (Fig. 10c). Since the

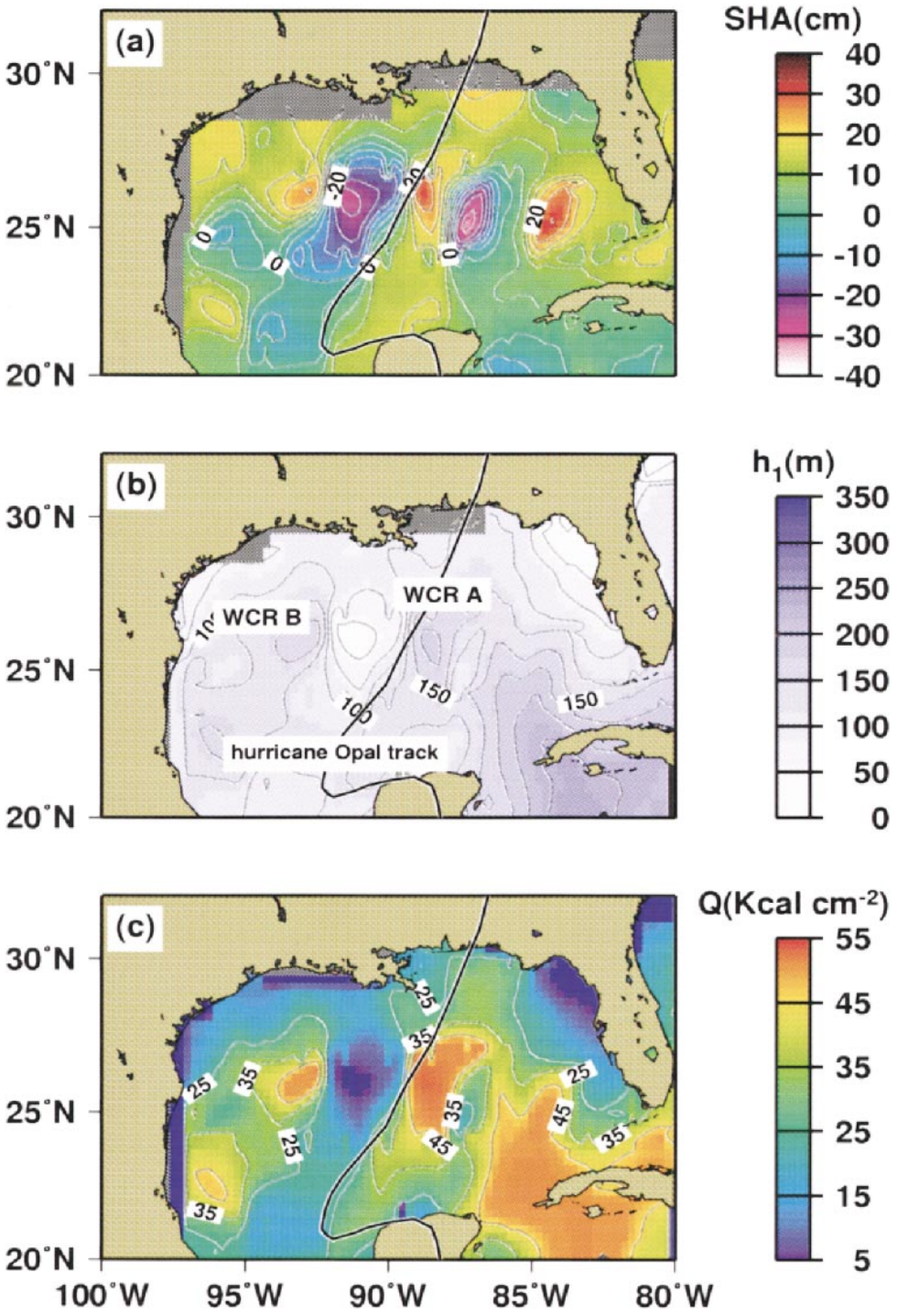

FIG. 9. (a) Surface height anomaly field (η' in cm) before the passage of Opal, (b) upper-layer thickness [$h_1(x, y, t)$ in m], and (c) upper-ocean heat content (Q in Kcal cm^2) relative to the depth of the 26°C isotherm. The contour intervals are (a) 10 cm, (b) 50 m, and (c) 10 Kcal cm^{-2}, respectively. Notice that the upper-layer thickness exceeds 200 m in the WCR regime.

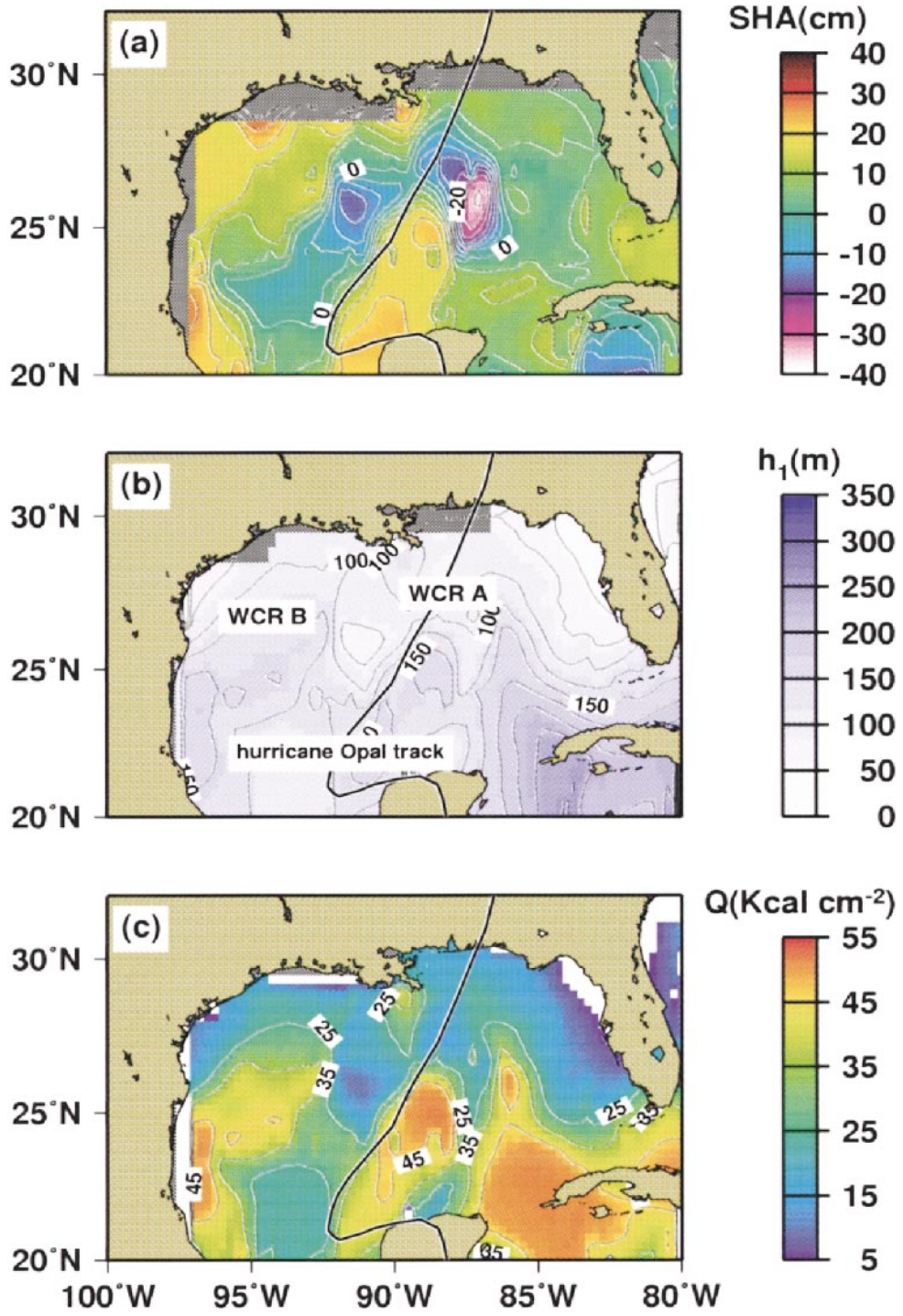

FIG. 10. Same as Fig. 9 except after Opal passage.

WCR is a product of the instability process associated with the Loop Current, the heat content in the Yucatan Straits has similar values. Although there is a substantial amount of heat remaining, the upper-ocean heat content decreased significantly during Opal's passage.

c. *Differences in estimated fields*

The decrease of the SHA values is approximately 20 cm between pre- and post-Opal states (Fig. 11a). The upper-layer thickness decreased by approximately 2ξ

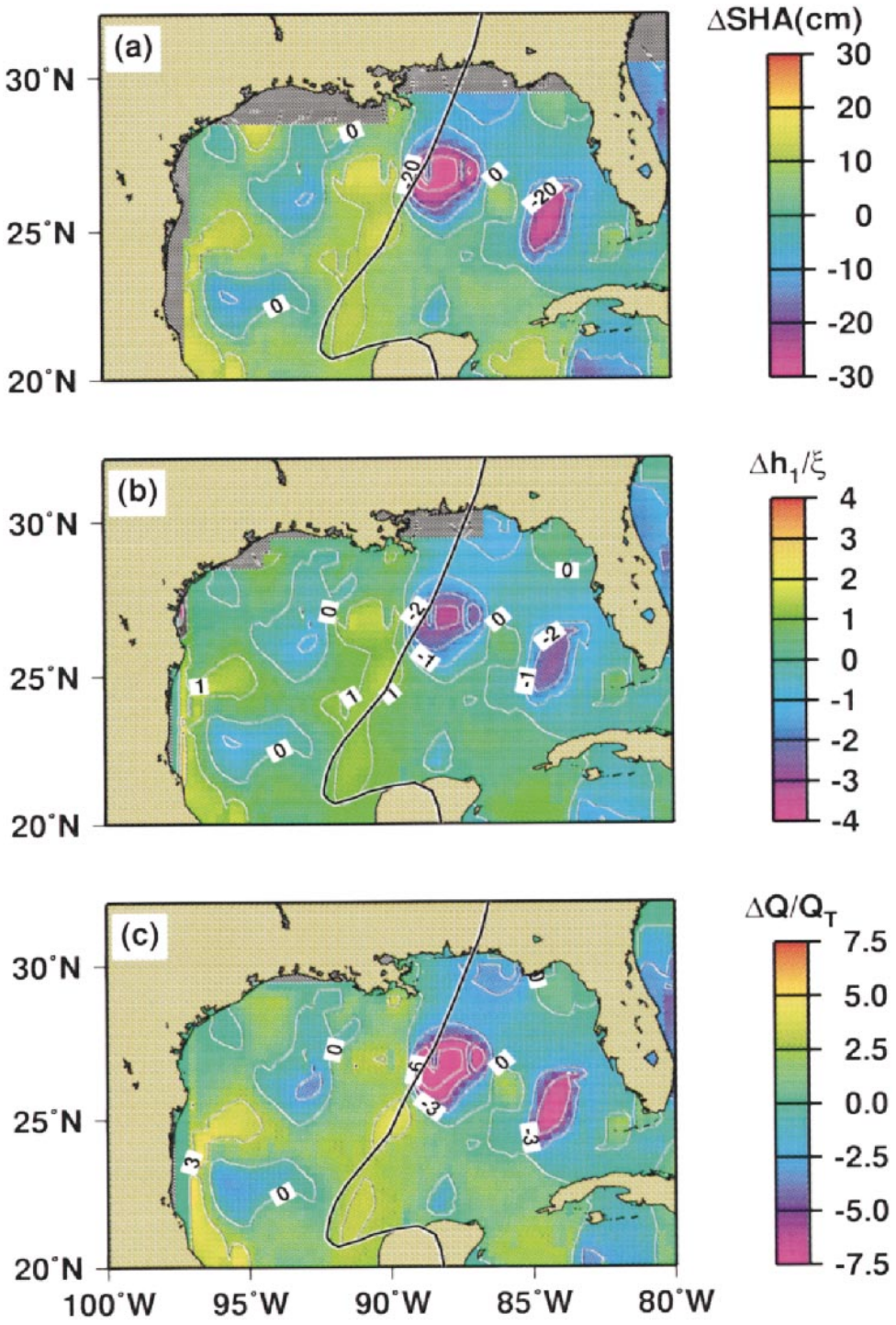

FIG. 11. The change in (a) surface height anomalies (cm), (b) upper-layer thickness normalized by ξ (22 m), and (c) heat content normalized by the Leipper and Volgenau (1972) estimate (Q_T = 4 Kcal cm^{-2}) found by differencing the pre-Opal and post-Opal fields.

(50 m) due primarily to Ekman divergence and the upwelling processes in the thermocline (Fig. 11b). There is also a net heat content loss in WCR A of approximately $6Q_T$ (where Q_T is the Leipper and Volgenau estimate required to sustain a tropical cyclone of 4 Kcal cm^{-2}), which equates to approximately 24 Kcal cm^{-2} over a 20-day period (Fig. 11c). However, this heat loss occurred over the 14-h period, which is borne out by

numerical guidance from a coupled atmosphere–ocean model (Hong et al. 2000).

The SST response detected by buoy 42001 (Fig. 4c) and AVHRR (Fig. 6d) suggested a change of 0.5°–1°C in the WCR area and 2°–3°C in the cold wake of Hurricane Opal including over the shelf where stratification is stronger. The evidence suggests that the ocean did lose a significant amount of heat during a time when Opal deepened and intensified from 965 to 916 hPa. Recent simulations using a coupled ocean–atmosphere model with a realistic basic state (i.e., eddy field) not only revealed similar SST changes, but also an associated increase in the surface heat flux (Hong et al. 2000), where approximately 60% of the intensity increase was ascribed to the WCR regime. Given the results reported by Bosart et al. (2000), it is concluded that the atmospheric and oceanic conditions must have been phase locked for this explosive deepening cycle of Opal over the WCR in the Gulf of Mexico.

d. Error analysis

The T/P altimeter cannot identify ring locations when they are located inside the diamond-shaped grid between ground tracks. Moreover, the altimeter will underestimate ring anomalies when the ground tracks cross the feature far from its center. The warm ring location relative to the altimeter ground track, and the deviation of the actual SST from the historical mean, both contribute to the computational heat content errors. Warm rings have a translation speed of a few kilometers per day (Elliot 1982; Cooper et al. 1990) and, along consecutive cycles, the altimeter ground track is juxtaposed over different parts of the ring. For rings propagating westward (i.e., Rossby wave dynamics), the SHA increases (decreases) as the center of the ring is approaching (receding from) the altimeter ground track. Therefore, at any given time, the altimeter underestimates the actual SHA of the ring. It is only when the altimeter ground track crosses the ring close to its center that the value of SHA is fairly close to the actual value. Moreover, the sampling periods of 9.9 days in T/P altimeter can also cause an underestimation of approximately 10% of the actual SHA value.

Based upon a series of images, the mean translation speed of rings, and specifically of WCR A, is approximately 5 km day^{-1}, which is within the range defined by Vukovich and Crissman (1986). Since consecutive altimeter passes are 10 days apart, this WCR is assumed to have translated approximately 50 km toward the west during that time. This propagation of the feature may represent a positive or negative change of 5–10 cm in the estimated SHA, which, in turn, yields maximum changes of 20 m in the upper-layer thickness estimate, 10 m in the H estimate, and 4 Kcal cm^{-2} in the Q estimates for an SST of 27°C. Clearly, these uncertainties are well below the signals found in the analysis of the remotely sensed images here.

e. Oceanic heat content versus surface heat flux

The total heat loss computed above is not all released to the atmosphere by air–sea fluxes. Entrainment mixing at the OPBL base generally accounts for 75%–90% of the cooling based on observations (Black 1983; Jacob et al. 2000), theoretical studies (Greatbatch 1983), and numerical results (Price 1981). Since Opal moved at speeds greater than 8 m s^{-1} during the acceleration phase, the time available for vertical ocean mixing of 4 h is short compared to the local inertial period of 27 h. Since in situ measurements were not acquired from airborne expendable current profilers (AXCPs), it is difficult to assess the net effect of entrainment heat fluxes induced by near-inertial current shears across the base of the OPBL (Sanford et al. 1987; Shay et al. 1998). These measurements would have provided ocean velocity and temperature structural variations to estimate entrainment heat fluxes induced by near-inertial current shear and advective tendencies (see Fig. 5). In warm baroclinic regimes, horizontal advection by geostrophic currents may also play a role in the OPBL heat balance during Opal as found in Hurricane Gilbert where 10%–15% of the heat budget in a WCR was due geostrophic advection (Jacob et al. 2000). Satellite-based ocean estimates from TOPEX/Poseidon and AVHRR from Opal were obtained from a two-week period prior and subsequent to passage allowing for the basic-state flows to contribute to the heat budget, compared to asynoptic ship-based measurements over three to four weeks (Leipper and Volgenau 1972).

It is unclear as to how much of the observed oceanic heat content change escaped to the atmosphere through the air–sea interface by latent and sensible heat flux. If the heat loss occurred over a period of 14 h as suggested by the simulations, the heat content loss of 24 Kcal cm^{-2} is approximately 20 kW m^{-2}. Given previous observational results that about 10%–15% of the cooling in the upper ocean is due to surface heat fluxes (Black 1983), estimated heat fluxes would range between 2000 and 3000 W m^{-2}. Interestingly, the numerical simulations from the coupled model indicated surface heat fluxes exceeding 2600 W m^{-2} (Hong et al. 2000). This equates to about 13% of the available upper-ocean heat was released to the atmosphere during Opal's encounter with the WCR, but larger than those found from buoy measurements (Cione et al. 2000). Caution has to be applied here because intensity changes are not always juxtaposed with the moored air–sea buoy network. Notwithstanding, the general agreement between observations and simulations suggests consistency in the estimates at least to first order.

The spatial scaling of the atmospheric and oceanic vortices remains an important consideration in the interactions. The horizontal scale associated with the positive vorticity core of the tropical cyclone is approximately $\pm 2R_{\max}$. In the Opal case, the initial $R_{\max}$ was about 40 km at 2000 UTC 3 October, whereas in the

area of maximum deepening the eye contracted to 25 km at 1000 UTC 4 October. The diameter of the vorticity maximum decreased from 160 to 100 km, a size comparable to the diameter of the WCR of about 200 km. While the tropical cyclone removes heat from the ocean over broad scales, a tropical cyclone moving over these deeper reserviors of high-heat content water will experience a substantial increase in the surface heat fluxes particularly in strong heat content gradient regimes. Thus, accurate measurements of air–sea fluxes with concurrent profilers in both fluids must be acquired to relate the inner and outer core wind and thermodynamic structures to this upper-ocean variability (Black and Shay 1998).

5. Concluding remarks

Satellite-based remote sensing estimates of the surface topography provide more information about the underlying ocean thermal structure when combined with historical and in situ measurements. Given an rms error of a few centimeters for the TOPEX/Poseidon altimeter, structures such as warm and cold rings, boundary currents, and fronts can be identified from the changes in the free surface elevation. Goni et al. (1997) demonstrates that the altimeter data is useful to study regimes rich in mesoscale variability, such as rings off the Agulhas retroflection area off South Africa. Time series of continuous spatial measurements of SHA provide the data to trace the paths of WCRs, and to estimate the upper-layer thicknesses and the baroclinic and barotropic transports within the context of a simple two-layer model.

Extraction of the heat content is an extension of hydrostatic dynamics in that warm (cold) features are elevated (depressed) with respect to the mean conditions. The two-layer ocean model is based on the depth of the 20°C isotherm, which separates the lower- from the upper-oceanic layer. Using historical hydrographic measurements, empirical relationships are determined from least square fits between the 20° and 26°C isotherm depths. Layer thicknesses relative to the depth of the 26°C isotherm derived from the SHA field when combined with mean temperature gradients provide crude synoptic estimates of the upper ocean's heat content. After the passage of Hurricane Opal, the upper-layer thickness changed by about 2ξ (50 m), which is consistent with the heat content decrease by $6Q_T$ (24 Kcal cm^{-2}) along the hurricane track during the approximate time of encounter of 14 h. If this time rate of change is used, the upper ocean lost approximately 20 kW m^{-2}. Given that the heat release from the ocean to the atmosphere based upon observations ranges between 10% and 15% (Black 1983), surface flux estimates presumably exceeded 2000 W m^{-2}. Numerical simulations of the coupled response over the WCR were in excess of 2600 W m^{-2} (Hong et al. 2000), or roughly 13%–15% of the observed cooling signals derived from TOPEX altimetry.

The net change of $6Q_T$ and this large surface heat flux were well above the threshold estimates to sustain cyclones (Leipper and Volgenau 1972). Indeed, caution has to applied to this threshold value given that upper-ocean processes such as advection and vertical shear are not explicitly included in the approach due to the lack of in situ measurements. Over the next few years, current and density profile measurements from AXCPs (Shay et al. 1992, 1998), mixed layer floats (D'Asaro et al. 1996), and possibly autonomous underwater vehicles (Smith et al. 1998) will have to be related to remotely sensed signatures of the SHA field especially in warm oceanic features to improve our understanding of these processes.

Central to this theme, important science issues are to investigate how much of the heat potential loss is due to (i) enhanced air–sea heat exchange, (ii) entrainment mixing at the OPBL base through shear instabilities, and (iii) horizontal advection. Since the time available for vertical mixing in the Opal case was short compared to the local inertial period (Greatbatch 1983), the entrainment heat fluxes may have not approached the limits found under quiescent conditions. In regions of a shallow OPBL, vigorous near-inertial current shear induce vertical mixing events by lowering the Richardson number to below criticality. Consistent with mixing length theory, more near-inertial shear is required in deeper WCR to lower the bulk Richardson number to below criticality. Such strong shear-induced mixing events do not usually occur at depths below 100 m as determined from previous measurements. In the case of slow moving or stationary storm, upwelling of the isotherms will also alter the WCR structure (Black 1983).

Jacob et al. (2000) has emphasized the importance of horizontal advection in the OPBL heat balance in a WCR during the passage of Gilbert. The WCR did not cool significantly, suggesting that additional heat was available for the APBL albeit at 4–5 $R_{\max}$ from the storm track. In the present case, the possibility exists that a large fraction of the heat may have been lost to the APBL via enhanced air–sea exchange process as supported by buoy-derived estimates and numerical simulations (Hong et al. 2000). Considerable uncertainty remains in the transfer coefficients that need further investigation. These results raise new questions about the upper ocean's role in modulating intensity changes in the tropical cyclones especially under favorable atmospheric conditions as found in Opal (Bosart et al. 2000).

Remotely sensed observations from TOPEX/Poseidon and AVHRR set the background conditions by detecting warm oceanic features and provide spatial context for oceanic and atmospheric observations acquired during NOAA Hurricane Research Division (HRD) flights. In addition, the enhanced SHA fields will be improved by blending TOPEX and European Remote Sensing Satellite (ERS) radar measurements. Pre- and

post-storm SHAs and SSTs observations will establish a database to determine relationships between these oceanic data and tropical cyclone observations where intensification is likely to occur from an oceanographic perspective. Locations of these areas of variability where warm mesoscale features dominate the circulation have been made available on a Web site for the forecasting and research communities. Finally, aircraft and buoy technology has now emerged to the point where air–sea interactions during these extreme events can be quantified with movable observing strategies that complements NOAA HRD research and National Hurricane Center reconnaissance missions. These measurements will allow coupled models to be tested to exploit deficiencies in parameterizations, to advance new ideas, and to isolate physical processes involved in the air–sea interactions (Hong et al. 2000). This approach will provide important insights into the ocean's role in modulating tropical cyclone intensity change (Marks et al. 1998).

Acknowledgments. LKS and GJJ appreciate support from ONR (through Grants N00014-93-1-0417 and N0014-95-1-0166) and the National Science Foundation (NSF) and NOAA (ATM-9714885) by the Mesoscale Dynamic and Large Scale Meteorology programs and Physical Oceanography programs at NSF under the auspices of the United States Weather Research Program. Dr. Kristina Katsaros, director of NOAA AOML, RSMAS Dean Otis Brown, and the RSMAS Remote Sensing Group continue to be supportive of these efforts. TOPEX altimeter data was provided by NASA/JPL. Vicki Halliwell, Ed Ryan, and Arthur Mariano (RSMAS) provided the high-resolution SST fields. T. Faber, S. D. Jacob, T. Cook, and S. Munro (NOAA) assisted in the manuscript preparation and calculations. We further appreciate the observation of Ivan Soares that NDBC buoy 42001 was located in the WCR during Opal's passage as part of his air–sea interaction project. Comments from two anonymous reviewers and the editor significantly improved the quality of the manuscript.

REFERENCES

Black, P. G., 1983: Ocean temperature changes induced by tropical cyclones. Ph.D. dissertation, The Pennsylvania State University, 278 pp. [Available from The Pennsylvania State University, University Park, PA 16802.]

——, and L. K. Shay, 1998: Observations of tropical cyclone intensity change due to air–sea interaction processes. Preprints, *Symp. on Tropical Cyclone Intensity Change,* Phoenix, AZ, Amer. Meteor. Soc., 161–168.

Bohren, C., and B. Albrecht, 1998: *Atmospheric Thermodynamics.* Oxford University Press, 402 pp.

Bosart, L., C. S. Velden, W. E. Bracken, J. Molinari, and P. G. Black, 2000: Environmental influences on the rapid intensification of Hurricane Opal (1995) over the Gulf of Mexico. *Mon. Wea. Rev.*, **128,** 322–352.

Cione, J. J., P. G. Black, and S. Houston, 2000: Surface observations in the hurricane environment. *Mon. Wea. Rev.*, **128,** 1550–1561.

Cooper, C., G. Z. Forristall, and T. M. Joyce, 1990: Velocity and hydrographic structure of two Gulf of Mexico warm core rings. *J. Geophys. Res.,* **95,** 1663–1679.

D'Asaro, E., D. M. Farmer, J. T Osse, and G. T. Dairiki, 1996: A Lagrangian float. *J. Atmos. Oceanic Technol.,* **13,** 1230–1246.

DeMaria, M., and J. Kaplan, 1994: Sea surface temperature and the maximum intensity of Atlantic tropical cyclones. *J. Climate,* **7,** 1324–1334.

Elliot, B. A., 1982: Anticyclonic rings in the Gulf of Mexico. *J. Phys. Oceanogr.,* **12,** 1292–1309.

Elsberry, R. L., T. Fraim, and R. Trapnell, 1976: A mixed layer model of the ocean thermal response to hurricanes. *J. Geophys. Res.*, **81,** 1153–1162.

Emanuel, K., 1986: An air–sea interaction theory for tropical cyclones. Part I: Steady-state maintenance. *J. Atmos. Sci.,* **43,** 585–604.

Garzoli, S. L., G. J. Goni, A. J. Mariano, and D. B. Olson, 1997: Monitoring the upper southeastern transports using altimeter data. *J. Mar. Res.,* **55,** 453–481.

Geisler, J. E., 1970: Linear theory on the response of a two-layer ocean to a moving hurricane. *Geophys. Fluid Dyn.,* **1,** 249–272.

Goni, G. J., S. Kamholtz, S. Garzoli, and D. B. Olson, 1996: Dynamics of the Brazil–Malvinas confluence based upon inverted echo sounders and altimetry. *J. Geophys. Res.*, **101** (7), 16 273–16 289.

——, S. L. Garzoli, A. Roubicek, D. B. Olson, and O. B. Brown, 1997: Agulhas ring dynamics from TOPEX/Poseidon satellite altimeter data. *J. Mar. Res.,* **55,** 861–883.

Greatbatch, R. J., 1983: On the response of the ocean to a moving storm: The nonlinear dynamics. *J. Phys. Oceanogr.,* **13,** 357–367.

Holland, G. J., 1997: The maximum potential intensity of tropical cyclones. *J. Atmos. Sci.,* **54,** 2519–2541.

Hong, X., S. W. Chang, S. Raman, L. K. Shay, and R. Hodur, 2000: The interaction between Hurricane Opal (1995) and a warm core eddy in the Gulf of Mexico. *Mon. Wea Rev.,* **128,** 1347–1365.

Jacob, D. S., L. K. Shay, A. J. Mariano, and P. G. Black, 2000: The 3D oceanic mixed layer response to Hurricane Gilbert. *J. Phys. Oceanogr.,* in press.

Kraus, E. B., and J. S. Turner, 1967: A one-dimensional model of the seasonal thermocline. II: The general theory and its consequences. *Tellus,* **1,** 98–105.

Leipper, D., and D. Volgenau, 1972: Hurricane heat potential of the Gulf of Mexico. *J. Phys. Oceanogr.,* **2,** 218–224.

Levitus, S., 1984: Annual cycle of temperature and heat storage in the world's ocean. *J. Phys. Oceanogr.,* **14,** 727–746.

Marks, F., L. K. Shay, and PDT-5, 1998: Landfalling tropical cyclones: Forecast problems and associated research opportunities. *Bull. Amer. Meteor. Soc.,* **79,** 305–323.

Maul, G., 1977: The annual cycle of the Loop Current. Part I: Observations during a one-year time series. *J. Mar. Res,* **35,** 29–47.

Namias, J., and D. R. Canyan, 1981: Large air–sea interactions and short period climatic fluctuations. *Science,* **214,** 869–876.

Palmen, E., 1948: On the formation and structure of tropical cyclones. *Geophysics,* **3,** 26–38.

Pielke, R. A., Jr., and R. A. Pielke Sr., 1997: *Hurricanes: Their Nature and Impacts on Society.* John Wiley and Sons, 279 pp.

Powell, M. D., and S. H. Houston, 1996: Hurricane Andrew's landfall in south Florida. Part II: Surface wind fields and potential real-time applications. *Wea. Forecasting,* **11,** 329–349.

Price, J. F., 1981: Upper ocean response to a hurricane. *J. Phys. Oceanogr.,* **11,** 153–175.

——, 1983: Internal wave wake of a moving storm. Part I: Scales, energy budget, and observations. *J. Phys. Oceanogr.,* **13,** 949–965.

Sanford, T. B., P. G. Black, J. Haustein, J. W. Feeney, G. Z. Forristall, and J. F. Price, 1987: Ocean response to a hurricane. Part I: Observations. *J. Phys. Oceanogr.,* **17,** 2065–2083.

Shay, L. K., 1997: Near-inertial wave energy fluxes forced by

tropical cyclones. Preprints, *22d Conf. Hurricanes and Tropical Meteorology*, Fort Collins, CO, Amer. Meteor. Soc., 437–438.

——, and S. W. Chang, 1997: Free surface effects on the near-inertial ocean current response to a hurricane: A revisit. *J. Phys. Oceanogr.*, **27,** 23–39.

——, P. G. Black, A. J. Mariano, J. D. Hawkins, and R. L. Elsberry, 1992: Upper ocean response to Hurricane Gilbert. *J. Geophys. Res.*, **97** (12), 20 227–20 248.

——, A. J. Mariano, D. S. Jacob, and E. H. Ryan, 1998: Mean and near-inertial ocean current response to Hurricane Gilbert. *J. Phys. Oceanogr.*, **28,** 858–889.

Smith, S., E. An, J. C. Park, L. K. Shay, H. Peters, and J. VanLeer, 1998: Submesoscale coastal ocean dynamics using autonomous underwater vehicles and HF radar. Preprints, *Second Conf. on Coastal Atmospheric and Oceanic Prediction and Processes*, Phoeniz, AZ, Amer. Meteor. Soc., 143–150.

Vukovich, F. M., and B. W. Crissman, 1986: Aspects of warm core rings in the Gulf of Mexico. *J. Geophys. Res.*, **91,** 2645–2660.

WAMDI Group, 1988: The WAM model—A third generation ocean wave prediction model. *J. Phys. Oceanogr.*, **18,** 1775–1810.